Combustion and Flame 229 (2021) 111397

Contents lists available at ScienceDirect

Combustion and Flame

journal homepage: www.elsevier.com/locate/combustflame

Identifying the contribution of rich-CO_2/H_2O gasification on the char conversion in typical atmospheres of chemical looping with oxygen uncoupling via single particle simulation

Chuanbao Zheng[1], Mingze Su[1], Haibo Zhao*

State Key Laboratory of Coal Combustion, School of Energy and Power Engineering, Huazhong University of Science and Technology, 1037 Luoyu Road, Wuhan 430074, China

ARTICLE INFO

Article history:
Received 17 April 2020
Revised 23 February 2021
Accepted 26 February 2021

Keywords:
Chemical Looping with Oxygen Uncoupling
Lean-O_2 combustion
Rich-CO_2 gasification
Rich-steam gasification
Particle-resolved simulation

ABSTRACT

Char conversion is an important but also complicated step during the combustion of solid fuels (*i.e.* coal and biomass) in chemical looping with oxygen uncoupling (CLOU). Potentially, both the lean-O_2 oxidation and rich-CO_2/H_2O gasification reactions of char contribute to the char conversion. However, the contribution degree of char gasification reaction has rarely been quantified in typical CLOU atmosphere. In this work, the single particle simulation is conducted to theoretically understand the effects of different operation conditions on the char conversion, and to identify the contribution degree of rich-CO_2/H_2O gasification in CLOU. A 10-step heterogeneous reaction mechanism is used for the gas-char reactions, and the random pore model is adopted to account for the evolution of porous char structure as well as its impact on reaction rates. The detailed conversion processes of chars with different sizes are simulated in various concentrations of gasification/oxidation agents and at different temperatures. The amounts of char consumed by lean-O_2 combustion, rich-CO_2 gasification, and rich-H_2O gasification are assumed to be proportional to the amounts of surface adsorbed species generated by char reacting with O_2, CO_2, and H_2O, and a formula to quantitatively calculate the relative contributions of the gasification reactions (both with CO_2 and steam) is finally proposed. The results indicate that the gasification reactions (occurring in the inner core of the char particle) hardly influence the oxidation reaction (dominating the heterogeneous reaction in the external layer of the char particle) under CLOU conditions. The CO_2-char gasification contributes less than 3% on the char conversion, while the contribution of H_2O-char gasification can even reach 2–18%. The char-H_2O gasification contributes more significantly (18% for 0.5 vol.% O_2, and 2% for 4 vol.% O_2) under the O_2-deficient conditions. Generally, the overall contribution of gasification reactions on the char conversion is between 1 and 20% in CLOU, which depends on the reaction temperature, gas composition, and char particle size.

1. Introduction

Chemical looping combustion (CLC) has attracted a lot of attention due to its inherent advantage of low-cost CO_2 capture, as realized by using lattice oxygen in oxygen carrier (OC) instead of O_2 in air for fossil fuel combustion [1–3]. The development of *in-situ* gasification CLC (*i*G-CLC) makes the use of solid fuels in chemical looping feasible, but the slow char gasification rate limits the whole *i*G-CLC process to some extent [4]. To address this issue, an alternative chemical looping process, as known as chemical looping with oxygen uncoupling (CLOU), was further proposed for solid fuel combustion. In CLOU, metal oxides (*e.g.*, CuO, Mn_2O_3, Co_2O_3, *etc.* [5–7]) with the capability of releasing molecular oxygen under O_2 deficient atmosphere, were selected as the potential OCs [8]. It was believed that the gaseous O_2 generated within CLOU could eventually contribute to a much higher char conversion rate, CO_2 capture efficiency, and combustion efficiency [9]. In a typical coal-derived CLOU process, the coal char particles are surrounded by the gas atmosphere of low O_2 concentration (< 5 vol.%) and high H_2O/CO_2 concentration (*e.g.*, 90 vol.% or even higher), where both combustion and gasification reactions could potentially contribute to the char conversion. It was generally believed that the coal char conversion in CLOU processes is dominated by the lean-O_2 combustion, while the potential contribution of the rich-CO_2 (or H_2O) gasification was rarely evaluated. In fact, according to the batch

* Corresponding author.
E-mail address: hzhao@mail.hust.edu.cn (H. Zhao).
[1] These authors contributed equally to this work.

https://doi.org/10.1016/j.combustflame.2021.111397
0010-2180/

fluidized-bed tests [10], when the steam concentration in the fluidization agent increased from 40 vol.% to 60 vol.%, an obviously promoted instantaneous char conversion rate could be observed, indicating the non-negligible contribution of char gasification reactions in CLOU. Therefore, the contribution of char gasification reactions in CLOU deserves to be clearly quantified.

Up to date, the effect of the CO_2/H_2O gasification reaction on the overall char consumption rate in oxy-char combustion has been widely studied [11–15]. Considering the significant endothermic characteristic of char reacting with CO_2/H_2O and the different physical properties of CO_2/H_2O in comparison with N_2 (such as the heat capacity and diffusion coefficient), the gasification reactions can adversely affect the oxidation rate by reducing the reaction temperature and O_2 concentration [16,17]. On the other hand, the gasification reactions can consume part of the char and thus compensate the negative effect (*i.e.*, the suppressed oxidation rate) to some extent. However, up to now, whether the gasification reaction can fully compensate its suppressing effect on the oxidation rate has not been determined, and there are different opinions in literatures.

With respect to the CO_2-char gasification, Hecht et al. [18] used the Surface Kinetics in Porous Particles (SKIPPY) code to investigate the effect of CO_2 on oxy-combustion of pulverized coal char at 1724 K with three different O_2 concentrations (12 vol.%, 24 vol.%, and 36 vol.%). Meanwhile, the pre-exponential factor for the CO_2 gasification reaction was assumed to be changed in sensitivity analysis. The simulation results indicated that the CO_2 gasification can promotes the overall carbon consumption rate at a low O_2 concentration (12 vol.%), but reduces the rate at a high O_2 level (36 vol.%) by greatly lowering the particle temperature. The O_2 concentration of 24 vol.% was determined as a balance point at which the decrease of the char oxidation rate was just offset by the additional carbon consumption via the gasification process. However, in another study by Hecht et al. [19], the carbon consumption rate was elevated by gasification reactions (both with H_2O and CO_2) and this phenomenon was independent of the oxygen concentration. Kim et al. [20] also concluded that the CO_2 gasification reaction always promoted the overall char conversion rate. In an O_2-deficient environment (*ca.* 5 vol.%), the char burnout time would be more significantly affected by the gasification reaction, *i.e.*, the gasification reaction contributed more to the carbon consumption. Tolvanen et al. [21] experimentally and numerically studied the combustion of two coal chars in a drop-tube reactor. The oxygen concentrations were 12 vol.% in either N_2 or CO_2 at 1123 K. As observed, the change from O_2/N_2 to O_2/CO_2 resulted in a slight decrease of char conversion rate while a more significant decrease in particle temperature (about 250 K). The differences attained from above studies may be ascribed to the different coal ranks [22], experimental conditions (such as particle size and reaction temperature [23]), and simulation models [24].

On the other side, the influence of H_2O-char gasification reaction has also been extensively studied. The experimental results from Li et al. [25] showed that, at the high temperature condition (1673 K), H_2O possessed an enhancing effect on the overall carbon conversion at low stoichiometric ratios (SR) of O_2 to fuel (SR < 1) but had an inhibiting effect on the overall carbon conversion when O_2 was rich (5 vol.%, and the stoichiometric ratio of O_2 to fuel is 2.5). Zhou et al. [26] investigated the combustion characteristics of single coal particle in O_2/N_2 and O_2/H_2O in a flow tube reactor at 1073 K and 21–50 vol.% O_2. It was found that replacing N_2 by H_2O could increase the combustion rate of coal char within the investigated O_2 concentration range. Chen et al. [27] provided a comprehensive review on the char conversion studies in recent years and pointed out that the char gasification may contribute more to the overall char conversion at lower O_2 concentrations. All these results suggest that the char gasification reaction is rather significant under O_2-deficient conditions.

The low concentration of O_2 (<5 vol.%, *e.g.*, the equilibrium oxygen partial pressure of the commonly used CuO/Cu_2O OC in CLOU is 4.3% at 950 °C [28,29]) and high concentrations of CO_2/steam is the typical gas atmosphere in CLOU. In our previous publication [30], we developed a single particle model to analyze the conversion characteristics of pulverized coal char in lean-O_2 and/or rich-CO_2 conditions. However, to the best of our knowledge, there is no systematic research on the effects of gas compositions, temperatures, particle sizes, *etc.*, on char conversion under the CLOU condition (lean O_2 and rich CO_2/H_2O). The relative contribution of CO_2/steam gasification to the overall char conversion in CLOU is either ignored or lack of quantitative analysis in previous studies. This paper aims to reveal the char conversion characteristics and CO_2/H_2O gasification contributions under the contest of CLOU. To this end, the particle-resolved simulation is conducted to investigate the char particle conversion in CLOU, based on the heterogeneous reaction mechanism developed by Tilghman et al. [31], and the homogeneous reaction mechanism extracted from GRI-Mech 3.0 [32].

2. Model description

In this paper, the single particle simulation is conducted to explore the conversion process of a spherical reacting porous particle in details, on the basis of the existing classic models for coal char combustion/gasification [19,31,33,34]. Heat and mass transfer inside (porous media) and outside (gas phase domain) the coal char particle are both considered. The reaction rate is described by a detailed chemical reaction kinetics scheme.

2.1. Governing equations

The mass conservation equation of the gas phase is described as follows:

$$\frac{\partial}{\partial t}(\rho\phi Y_k) + \frac{1}{A}\frac{\partial}{\partial r}(\rho V_k A Y_k) = \dot{s}_k W_k \sigma_r + \dot{\varpi}_k W_k \phi \tag{1}$$

where, ρ is the density of gas phase (kg/m^3); ϕ is the local void fraction; Y_k is the mass fraction of the k^{th} species; $A = 4\pi r^2$, is the area normal to the radial direction (m^2); V_k and W_k are the diffusion velocity (m/s) and molar weight (kg/mol) of the k^{th} species, respectively; $\dot{s}_k$ is the molar production rate of the k^{th} species per unit area by heterogeneous reactions (mol/(m^2·s)) and $\dot{\varpi}_k$ is the molar production rate of the k^{th} species per unit volume by homogeneous reactions (mol/(m^3·s)); σ_r is the specific surface area per unit space volume (m^2/m^3).

The energy conservation equation is governed by:

$$\frac{\partial}{\partial t}(\rho\phi\bar{h} + \rho_{tr}(1-\phi)h_p) + \frac{1}{A}\frac{\partial}{\partial r}\sum_{k=1}^{K_g}(\rho V_k A Y_k h_k) + \frac{1}{A}\frac{\partial}{\partial r}\left(-\lambda_t A\frac{dT}{dr}\right) = -\sum_{k=1}^{K_g}\dot{\varpi}_k W_k \phi h_k - \sum_{k=1}^{K_{tot}}\dot{s}_k W_k \sigma_k h_k \tag{2}$$

where, $\bar{h}$, h_p and h_k are the enthalpy (kJ/kg) of the gas mixture, char particle and k^{th} species, respectively; ρ_{tr} is the true density of char particle (kg/m^3); K_g is the total number of gas-phase species; $\lambda_t = \lambda\phi + \lambda_p(1-\phi)$, is the total thermal conductivity (W/(m·K)); λ is the mixture-averaged gas thermal conductivity; λ_p is the particle thermal conductivity; K_{tot} is the total number of the gas, bulk, and surface species; It should be pointed that, the radiation source term is not considered in this work, since the char particle in fluidized bed reactor is almost entirely obscured by other particles with nearly the same temperature [30].

Table 1
Correlation equations involved in this model.

Consumption rate equation of solid phase:
$\frac{d\rho_{ap}}{dt} = \dot{s}_{C(B)}\,\sigma_r W_C$
Overall effective diffusion coefficient:
$\frac{1}{D_{eff}} = \frac{1}{D_{km,eff}} + \frac{1}{D_{K,k,eff}}$
$D_{K,k,eff} = \frac{\phi}{\tau} \times \frac{2r_{pore}}{3}\sqrt{\frac{8RT}{\pi W_k}}\; r_{pore} = \frac{2rf\phi}{\rho_{ap}S}$
Correlations of the morphology parameters:
$\sigma_r = \sigma_{r,0}(1-x_C)\sqrt{1-\psi\ln(1-x_C)}$[35]
$\phi = 1 - \frac{\rho_{ap}}{\rho_{tr}}\; x_C = 1 - \frac{\rho_{ap}}{\rho_{ap,0}}$

Here, $^*\rho_{ap}$ is the apparent density of the char particle (kg/m^3); D_{eff} is the overall effective diffusion coefficient; $D_{km,eff}$ is the effective bulk diffusion coefficient. $D_{K,k,eff}$ is the effective Knudsen diffusion coefficient, τ is the tortuosity of the particle; r_{pore} is the average pore radius (m); rf is the surface roughness factor; ϕ is the local void fraction; $\sigma_{r,0}$ is the initial specific surface area per unit space volume (m^2/m^3).

The heterogeneous reaction mechanism used in the model involves the transformation of surface species, and the surface site species conservation equation can be expressed as [31]:

$$\frac{dZ_k}{dt} = \frac{\dot{s}_k o_k}{\Gamma} - Z_k\frac{S_0^2}{S}\left(\frac{S^2}{S_0^2} - \frac{\psi}{2}\right)\dot{s}_{C(B)} W_C \tag{3}$$

where, k is surface species; Z_k is the site fraction of k^{th} surface species, and $\sum_{i=1}^{K_{surf}} Z_i = 1$, K_{surf} is the total number of surface species; o_k is the site number occupied by surface species k; Γrepresents the site density (mol/m^2); $\psi$is the structural parameter; S is the specific surface area (m^2/kg); S_0 is the initial specific surface area (475 m^2/kg in this work); $\dot{s}_{C(B)}$ is the mole production rate of C(B) per unit area through heterogeneous reactions (mol/(m^2·s)); W_C is the molar weight of the carbonaceous material.

The other equations that used in this model are listed in Table 1, and more details about this model can refer to our previous publication [30].

The conversion process of char with O_2, H_2O, and CO_2 involves the internal and external heat and mass transfer, as well as complicated homogeneous and heterogeneous reactions. In order to describe the char conversion process, different models have been established in literatures. Mitchell et al. [34] developed a model to successfully predict the changes of physical properties of the pulverized coal char particles during combustion. In this model, the lumped parameter method was adopted by assuming that the thermal conductivity of char particle was sufficiently large. Moreover, the external gas diffusion was considered only by a boundary condition using a simple correlation. Hecht et.al [19] used the SKIPPY model to explore the effects of CO_2 and H_2O gasification reactions on oxy-combustion of coal char. In the SKIPPY model, the heat and mass transfer (both internal and external diffusions) and homogeneous reactions (described by GRI-3.0) have been well considered. However, as both the oxidation and gasification reactions were treated as an adsorption-limited process, the effect of the competition between gasification and oxidation reactions cannot be carefully considered from the reaction mechanism aspect. To address this issue in existing models, we try to develop the present model to describe the competition between gasification and oxidation reactions, from not only the particle scale (porous structure) but also the scale of reacted surface (reactive site). In fact, to the best of our knowledge, the developed model is the only one in literatures that can consider the competition between the gasification and oxidation reactions simultaneously from the above two scales.

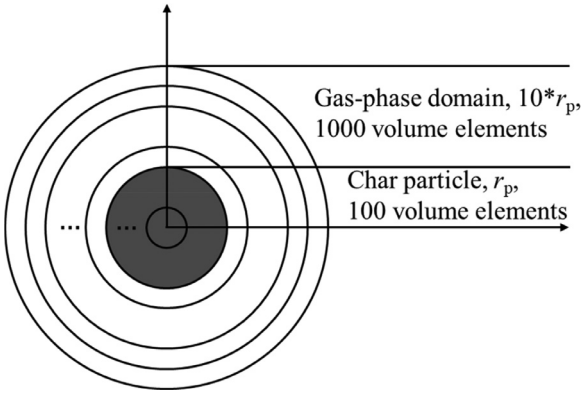

Fig. 1. Schematic view of the char particle and its external gas-phase domain.

Table 2
A simplified version of heterogeneous reaction kinetics of Wyodak coal char [31].

	Reaction	A	E(cal/mol)
R1	$2C(S)+H_2O \leftrightarrow C(H)+C(OH)$	2.10×10^{16}	25,095.60
R2	$C(OH)+C(S) \leftrightarrow C(O)+C(H)$	4.10×10^{15}	19,141.46
R3	$C(H)+C(H) \leftrightarrow 2C(S)+H_2$	1.40×10^{15}	16,013.38
R4	$C(O)+C(B) \rightarrow CO+C(S)$	1.55×10^{10}	59,629.54
R5	$CO_2+C(S) \leftrightarrow C(O)+CO$	3.70×10^{09}	38,479.92
R6	$C(B)+2C(S)+O_2 \rightarrow C(O)+CO+C(S)$	5.00×10^{20}	35,850.86
R7	$2C(S)+O_2 \rightarrow C_2(O_2)$	4.00×10^{17}	22,227.53
R8	$C(S)+C(B)+C(O)+O_2 \rightarrow CO_2+C(O)+C(S)$	1.50×10^{17}	18,642.45
R9	$C(S)+C(B)+C(O)+O_2 \rightarrow CO+2C(O)$	2.10×10^{17}	24,617.59
R10	$C(B)+C_2(O_2) \rightarrow CO_2+2C(S)$	1.26×10^{09}	38,293.50

*The unit of A is (mol, cm, s) based. The original parameters are converted according to the standard format of CHEMKIN input.

2.2. Mesh and boundary conditions

The schematic view of the computational domain is shown in Fig. 1. A spherical char particle with the initial radius of r_p is divided into 100 concentric annular volume elements. The external gas-phase domain is set as $10r_p$ (*i.e.*, 1000 vol elements).

The initial conditions ($t = 0$) are set as: $Y_{N_2} = 1, Y_{other} = 0; Z_{C(S)} = 1; T_p = T_{bulk}$. The zero-gradient boundary condition is set for the particle center ($r = 0$), while the boundary condition for the outermost concentric element is established as: $T = T_{buik}; Y_i = Y_{buik}$.

2.3. Reaction mechanism

In this work, the reaction mechanism developed by Tilghman et al. [31] is adopted to describe the heterogeneous reactions involved in the char particle conversion process, as shown in Table 2. C(S) represents the free carbon site, C(B) denotes the carbon atom in solid bulk phase, C(H), C(OH), and C(O) are the adsorbed surface species related to H, OH, and O, respectively. $C_2(O_2)$ is the O_2 molecules adsorbed on two adjacent C(B). According to the results of Tilghman et al. [31], the quantities of hydrocarbon species and oxygen-containing hydrocarbon compounds generated in the heterogeneous reactions are few, and the effect of these compounds on char conversion is negligible. Therefore, the heterogeneous elementary reactions containing hydrocarbon species and oxygen-containing hydrocarbon compounds are eliminated to save computational costs in this study. Simulation results also show that this simplification does not affect the accuracy of the model (as will be shown in Section 3.1). The homogeneous chemistry is extracted from the well-known GRI-Mech 3.0 mechanism [32], including the oxidation reactions of flammable species (H_2, CO) generated from heterogeneous and homogeneous reactions, and the water gas shift reaction.

Table 3
Simulation cases for this study.

Case #	Gas temperature (K)	Particle diameter (μm)	Molar fraction of O_2 (mol%)	Molar fraction of H_2O (mol%)	Molar fraction of CO_2 (mol%)
1	1223	100	1	99	0
2	1223	100	1	0	99
3	1223	100	1	50	49
4*	1223	100	1	0	0
5	1223	100	1	10	89
6	1223	100	1	30	69
7	1223	100	1	70	29
8	1223	100	1	90	9
9	1223	100	0	50	50
10	1223	100	0.5	50	49.5
11	1223	100	2	50	48
12	1223	100	3	50	47
13	1223	100	4	50	46
14	1173	100	1	50	49
15	1273	100	1	50	49
16	1223	200	1	50	49
17	1223	300	1	50	49

* N_2 is chosen as balance gas in Case 4.

It should be noted that for the desorption reactions (R4 and R10), the distributed activation energy method adopted in ref. [31] is not applicable in the CHEMKIN version that we use. Factually, the series-type distributed activation energy distribution is used to get the effective reaction rate coefficient ($k_{i,\mathrm{eff}}$), and $k_{i,\mathrm{eff}}$ can be expressed as [36]:

$$k_{i,\mathrm{eff}} = \int_0^\infty k_i(E) f(E) \mathrm{d}E \tag{4}$$

where $f(E)$ is the Gaussian distribution function, and it is used to describe the distribution of activation energies for the adsorbed species on the carbonaceous material.

$$f(E) = \frac{1}{\sigma\sqrt{2\pi}} \exp\left[-\frac{1}{2}\left(\frac{E-\bar{E}}{\sigma}\right)^2\right] \tag{5}$$

According to the above calculations, $k_{i,\mathrm{eff}}$ at different temperatures are determined. Then, the new activation energy and pre-exponential factor shown in Table 2 can be determined by Arrhenius fitting.

In the real CLOU condition, the oxygen release process of the OC will be significantly affected by its surrounding atmosphere and the internal diffusion of O_2 in the OC particle. However, this is an extremely complex process, which is beyond the scope of the present study and thus will not be discussed here.

Generally, considering that the OC is easily to sinter at high temperature while the low temperature condition is not conducive to the reaction rates (both for the char conversion and oxygen release of the OC), the reasonable operation window for CLOU is 1173–1273 K. On the other hand, the O_2 concentration in CLOU is usually lower than 5 vol.%. The concentration range of steam and/or CO_2 is relatively wide, which depends on the operation conditions. Moreover, in order to attain a high carbon conversion rate and high carbon capture efficiency, the coal/char particle size should not be too large, and the size range of 100–300 μm is reasonable. In combination with the aforementioned considerations, the simulation conditions in this work are listed in Table 3.

2.5. Relative contributions

Based on the heterogeneous reaction mechanism, the reactions of O_2 and CO_2/steam with char are initiated with the adsorption of oxygen and CO_2/steam on the active sites to yield adsorbed O species (C(O)), and then generates CO through R4. For the used reaction model, one can monitor the rate of R4, but cannot identify whether the consumed C(O) is from CO_2/steam gasification or O_2 oxidation. Therefore, the relative contributions of gasification/oxidation reactions cannot be distinguished. In order to calculate the relative contributions of CO_2/steam gasification to the overall char conversion, a hypothesis is adopted in this work: the amounts of char consumed by O_2, CO_2, and steam that through R4 are proportional to the amounts of C(O) that are generated by char reacting with O_2, CO_2, and steam, respectively. Karlström et al. [37] confirmed that the CO desorption occurred in the same way regardless of whether the char carbon reacts in O_2, CO_2, or H_2O, which provided a theoretical basis for this hypothesis. Based on this hypothesis, the following formula is proposed to calculate the relative contributions of gasification reactions:

$$\Omega = \frac{\mathrm{C}_{\text{consumed through C(O)}}}{\mathrm{C}_{\text{total consumption}}} \times \frac{\mathrm{CO}_{\text{generated from } H_2O/CO_2}}{\mathrm{C(O)}_{\text{total generation}}} \tag{6}$$

All the unknown quantities in Eq. (6) can be calculated by integrating the reaction rate of heterogeneous reactions over particle burn-out time, as:

$$\mathrm{C}_{\text{total consumption}} = \int_0^{t_\mathrm{b}} (R_{4,t} + R_{6,t} + R_{8,t} + R_{9,t} + R_{10,t})\mathrm{d}t \tag{7}$$

$$\mathrm{C}_{\text{consumed through C(O)}} = \int_0^{t_\mathrm{b}} R_{4,t}\mathrm{d}t \tag{8}$$

$$\mathrm{C(O)}_{\text{total generation}} = \int_0^{t_\mathrm{b}} (R_{2,t} + R_{5,t} + R_{6,t} + R_{9,t})\mathrm{d}t \tag{9}$$

$$\mathrm{C(O)}_{\text{generated from steam}} = \int_0^{t_\mathrm{b}} R_{2,t}\mathrm{d}t \tag{10}$$

$$\mathrm{C(O)}_{\text{generated from } CO_2} = \int_0^{t_\mathrm{b}} R_{5,t}\mathrm{d}t \tag{11}$$

$$R_{i,t} = \sum_0^k r_{i,k,t} \tag{12}$$

where i is the heterogeneous reaction number, t_b is the char particle burn-out time, k is the total number of volume elements at time t, and $r_{i,k,t}$ is the reaction rate of heterogeneous reaction i in the volume elements k at time t (mol/s), $R_{i,t}$ is the overall reaction rate of heterogeneous reaction i at time t (mol/s).

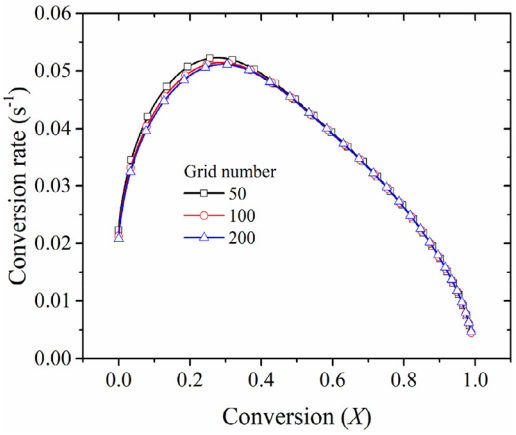

Fig. 2. The char conversion rates for three different grid resolutions. d_p = 100 μm, T_{gas} = 1223 K, 1 vol.% O_2/50 vol.% H_2O/49 vol.% CO_2.

3. Results and discussion

3.1. Grid independence analysis and model validation

3.1.1. Grid independence analysis

In the part, three simulations with different choice of discretisation parameter (grid number for char particle: 50, 100 or 200) are carried out to demonstrate that the main simulation results (*e.g.*, char conversion X) do not change with spatial resolution. Here, the char particle is spatially divided into 50, 100 or 200 concentric annular volume elements (corresponding to grid number for char particle of 50, 100, 200, respectively). As shown in Fig. 2, the char conversion rates obtained by three sets of grid system are almost overlapped with each other, which suggests that the spatial discretisation parameter (100 volume elements for char particle) chosen in the work is sufficient and reasonable.

3.1.2. Model validation

In order to validate the numerical code, the oxidation process of a char particle under typical zone II condition (T_{gas} = 1150 K, x_{O2} = 6 vol.% or P_{O2} = 0.06 atm, d_p = 100 μm) [34] are simulated. The kinetics parameters used in the simulation are derived from ref. [34], and Table 4 presents the physical properties of the char particle. The normalized diameter (D_p/D_{p0}), apparent density (ρ_p/ρ_{p0}), and specific surface area (S_{gp}/S_{gp0}) *vs.* conversion (X) are plotted in Fig. 3. Generally, both the detailed profiles of char physicochemical properties as a function of conversion and the macroscopic characteristic variable (such as the time required for the char particle to reach 90% conversion ($t_{90\%}$), 10.8 s ([19]) *vs.* 11.5 s (this work)) agree well with the available simulation results.

In order to validate the reliability of the heterogeneous reaction mechanism adopted, a series of numerical simulations have been conducted at different gas compositions and temperatures, with the internal diffusion effect being neglected (the details about

Table 4
Physical properties of the char particle in validation for numerical code [34].

Parameters	Values
Γ (mol/m^2)	1.08 × 10^{-4}
$\sigma_{r,0}$ (m^2/m^3)	2.47 × 10^8
τ (-)	3.0
ψ (-)	3.0
Δt (s)	1.0 × 10^{-5}
λ_p (W/mK) [19]	1.33
ρ_{tr} (kg/m^3)	1333.3
$\rho_{ap,0}$ (kg/m^3)	1000

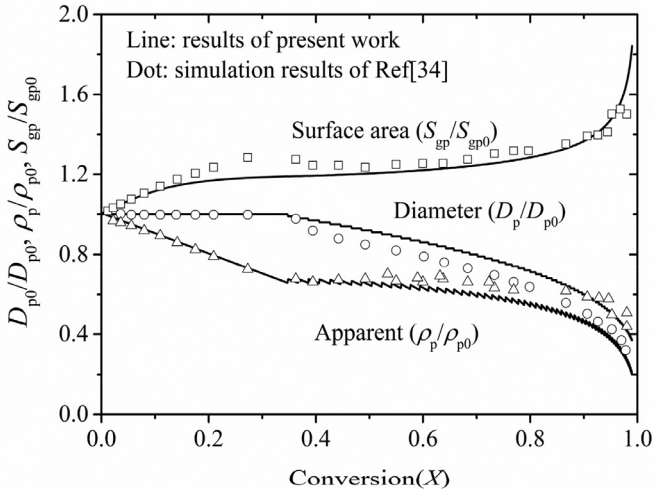

Fig. 3. Model/simulation validation for the numerical code. The reference data (hollow circle, hollow square and hollow triangle) is from ref. [34]. (T_{gas} = 1150 K, P_{O2} = 0.06atm).

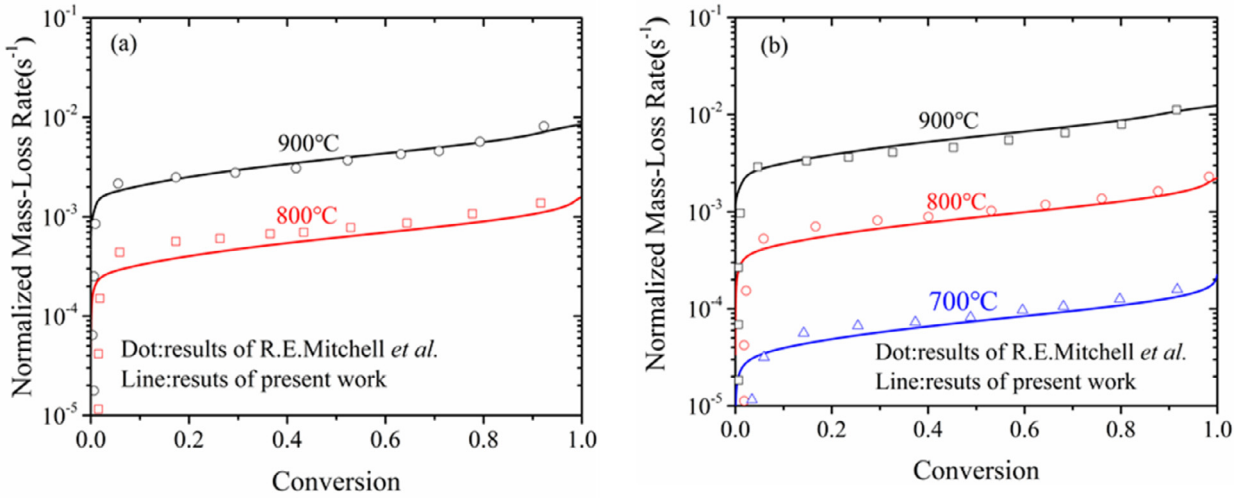

Fig. 4. Model/simulation validation for the char-H_2O reaction mechanism. The reference data is from ref. [31]. (a): 10%H_2O/N_2, (b): 20%H_2O/N_2,.

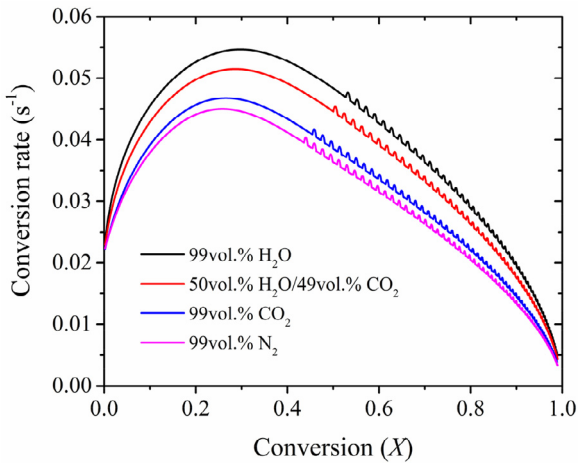

Fig. 5. The char conversion rate under different fluidizing agents. (T_{gas} = 1223 K, d_p = 100 μm, 1 vol.% O_2).

Table 5
Physical properties of the char particle in validation for heterogeneous reaction mechanism [31]. These char parameters are also used in the following simulations in this paper.

Parameters	Values
Γ (mol/m^2)	1.08 × 10^{-4}
$\sigma_{r,0}$ (m^2/m^3)	2.66 × 10^8
τ (-)	3.0
ψ (-)	8.0
Δt (s)	1.0 × 10^{-5}
λ_p (W/mK) [19]	1.33
ρ_{tr} (kg/m^3)	1302
$\rho_{ap,0}$ (kg/m^3)	560

the validation of numerical code have been described in our previous publication [30]). Table 5 provides the char particle properties used in this validation step. The mechanism of char reacts with CO_2 and O_2 has been well validated in our previous work [30]. Figure 4 compares the normalized mass loss rate available in ref. [31] with the simulation results of this work under different H_2O compositions and reaction temperatures. Generally, the small difference between the two sets of data (the simulation data in this work *vs*. the reference data in ref. [31]) is acceptable, and the slight difference is ascribed to the different model and simulation details. Therefore, it can be concluded that the numerical code and heterogeneous reaction mechanism are reasonable in this work.

It is noticed that the apparent density profile in Fig. 3 is jagged. Factually, this phenomenon has nothing to do with the resolution in time domain. In this paper, the particle diameter evolution

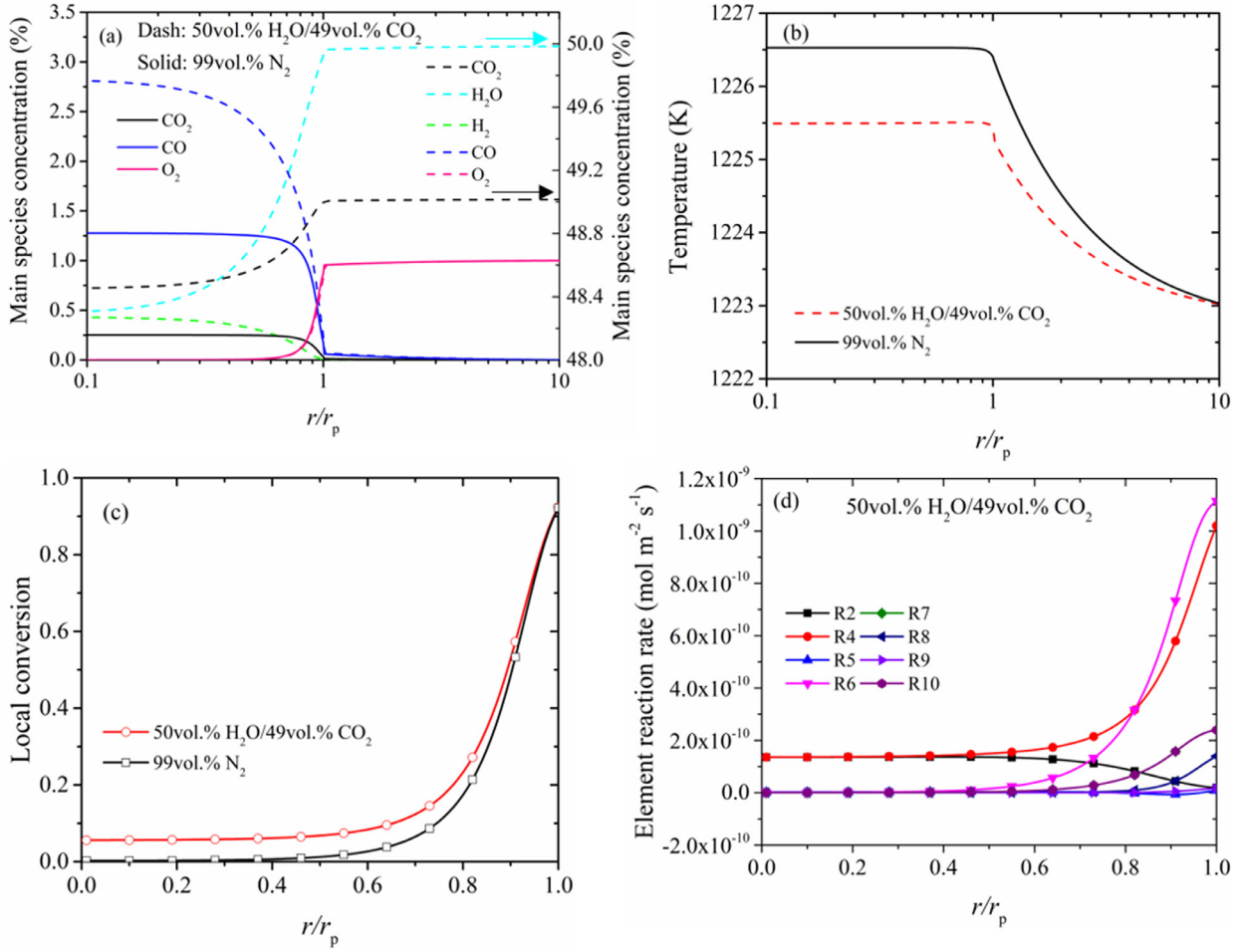

Fig. 6. Species profiles (a), particle temperatures (b), local conversion (c), and elementary surface reaction rates (d) as a function of normalized radial distance at t = 8 s. r_p is the initial particle radius, and r is the distance between the local point and the center of the particle, and r/r_p = 1 corresponds to the char surface. (T_{gas} = 1223 K, d_p=100 μm, 1 vol.% O_2).

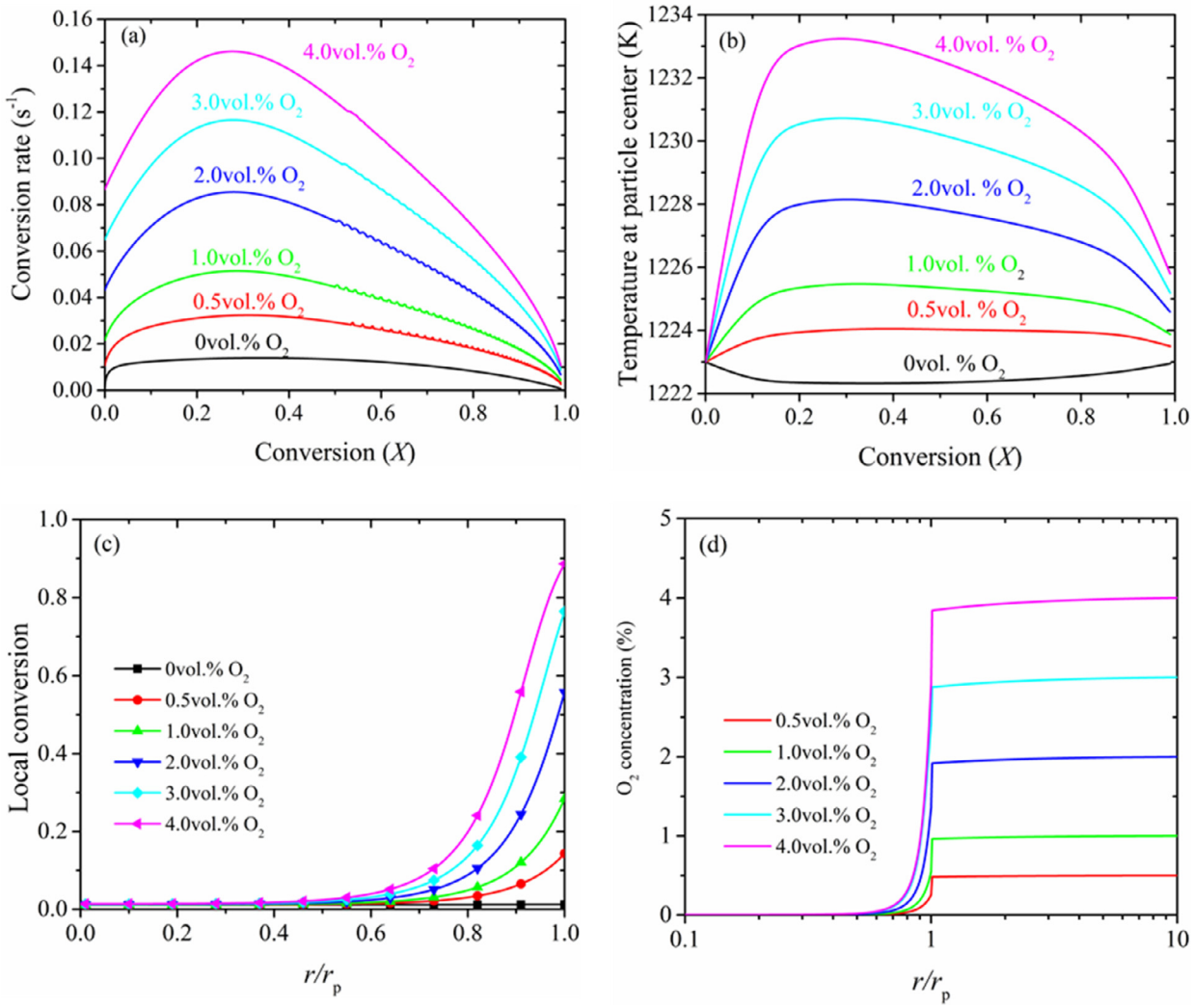

Fig. 7. Char conversion characteristics at different O_2 concentrations at t = 2.5 s. (T_{gas} = 1223 K, d_p = 100 μm, 50 vol.% H_2O, CO_2 as balance gas).

during the char particle conversion process is considered. To achieve this goal, the char particle is divided into 100 vol elements. And when the local conversion reaches 99.5%, the solid volume element is converted into gas phase element at the next time step. In other words, there is a step drop in the particle diameter and weight while the outmost volume element dismisses. In the meanwhile, there is no zig-zag for the apparent density and conversion rate (see the following figures) for overall conversions up to about 0.35 because in this stage the particle size does not decrease. There are two ways to dismiss or weaken the zig-zags: (1) elevate the threshold value for volume conversion; (2) divide the particle into more volume elements.

3.2. The effects of gasification reactions on char conversion

In this section, the char conversion characteristics under the conditions with different fluidizing gas agents (1 vol.% of O_2 together with rich CO_2, rich H_2O, hybrid CO_2/H_2O or N_2 as balance gas) are firstly simulated to reveal the effects of gasification reactions on char conversion. As shown in Fig. 5, it can be found that the existence of gasification agents (*i.e.*, steam and/or CO_2) can accelerate the char consumption in comparison with the case "1 vol.% O_2 + 99 vol.% N_2". Due to the higher chemical activity of H_2O than CO_2 towards char, the char conversion rate is obviously promoted with the increase of steam concentration.

The main species profiles and particle temperatures at t = 8 s under the above simulation conditions (as shown in Fig. 5) are plotted in Fig. 6. According to previous studies, it is generally believed that the gasification reaction affects the oxidation reaction in two aspects: reducing the particle temperature and affecting the external diffusivity of O_2 [11]. With respect to the char particle temperature, due to the exothermic nature of the reaction of O_2 with char, the particle temperature will slightly increase in contrast to ambient temperature. But the existence of gasification reaction (in the case "1 vol.% O_2+50 vol.% H_2O+49 vol.% CO_2") leads to a decrease of about 1 K in the particle temperature (Fig. 6b) in comparison with that in the case "1 vol.% O_2+99 vol.% N_2". While for the O_2 concentration at the particle surface and in the bulk atmosphere, no obvious difference is found for the two simulation cases, indicating that the influence of different gasification agents on the external diffusion of O_2 is not significant for the conditions studied. In fact, O_2 has different diffusion coefficients in different media. For example, the O_2 diffusion coefficient is 2.26 cm^2/s in N_2 while it is 1.90 cm^2/s in CO_2 at 1200 K [38]. To some extent, the local O_2 concentration at the particle surface (not the solid phase but the gas-phase zones close to char particle) depends on not only the O_2 diffusion from the bulk atmosphere to the particle surface

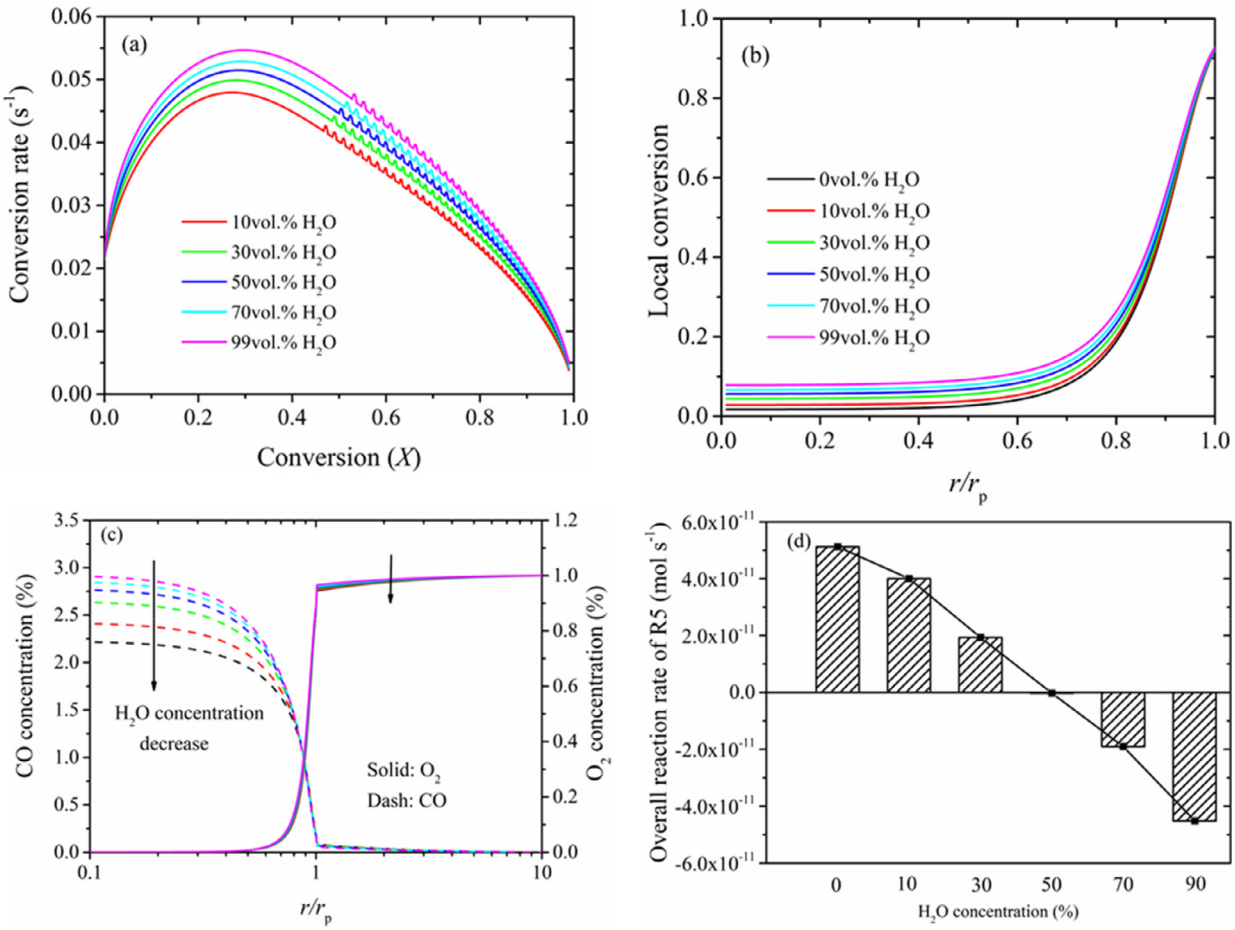

Fig. 8. Char conversion characteristics at different steam concentrations at t = 8 s. (T_{gas} = 1223 K, d_p = 100 μm, 1 vol.% O_2, CO_2 as balance gas).

but also the consumption by the oxidation of char/combustible gas species (H_2, CO, *etc.*). In this study, the overall oxidation reaction is hardly affected by external effect due to the relatively low reaction temperature and relatively small particle size. Based on the above analysis, it can be concluded that the influence of gasification reactions on oxidation reaction is minimal and can be ignored under the CLOU conditions. In addition, we notice that both CO_2 and H_2O maintain relatively high concentrations in the particle center as shown in Fig. 6a, which indicates that the influence of internal diffusion for these two species on gasification reaction is not significant under the investigated reaction temperature range.

Due to the higher chemical activity and lower concentration, O_2 is rapidly consumed at the particle surface and the O_2 concentration is close to 0 inside the particle, which indicates that the oxidation occurs mainly within the particle. Therefore, the conversion of char particle mainly takes place at the surface of the particle at these conditions, and the conversion inside the particle is close to 0 when gasification agent does not exist in the bulk gas phase, as shown in Fig. 6c (the local conversion of char particle at t = 8 s). When both lean-O_2 combustion and rich CO_2/H_2O gasification reactions are present, the local char conversion inside the particle is obviously improved. But at the surface of the particle, there is no obvious difference in the local conversion between the two conditions. This indicates that the gasification reaction mainly occurs in the interior of the particle, while the oxidation reaction mainly occurs at the exterior of the particle. Figure 6d presents the elementary surface reaction rates at t = 8 s, which are helpful to further understand the char conversion characteristics. All the reactions involving O_2 occur only at the surface ($0.5r_p < r \leq r_p$). According to our previous analysis [30], O_2 can preferentially occupy the active sites at the char particle surface, which inhibits the gasification reaction. Inside the char particle ($0 \leq r < 0.5r_p$), the rates of R6 - R10 (related to oxidation reaction) are close to 0 (because the O_2 concentration is close to 0), indicating that the conversion inside the particle is mainly contributed by the gasification reactions. And it should be noted that the rate of R4 (desorption of C(O)) almost equals to that of R2 (generation of C(O) by H_2O gasification), indicating that H_2O gasification reaction dominates the gasification process inside the char particle (because H_2O is more reactive than CO_2 [39]).

In the following part, a series of numerical simulations are conducted to understand the effects of O_2 concentration, steam concentration, reaction temperature, and particle size on char conversion by the single factor analysis.

3.3. The effects of O_2 concentration on char conversion rate

Firstly, the influence of oxygen concentration is analyzed. Figure 7a compares the total reaction rates of various O_2 concentration levels in the range 0–4 vol.% at a gas temperature of 1223 K, and the char particle size is 100 μm. As expected, the char conversion rate is significantly promoted with the increase of O_2 concentration. In comparison with the pure gasification condition (0 vol.% O_2), even only 0.5 vol.% of O_2 is present in the reactive atmosphere, the conversion rate of char can still be greatly enhanced, indicating that CLOU is indeed a good solution for the rate-limiting step (char conversion) existing in *i*G-CLC.

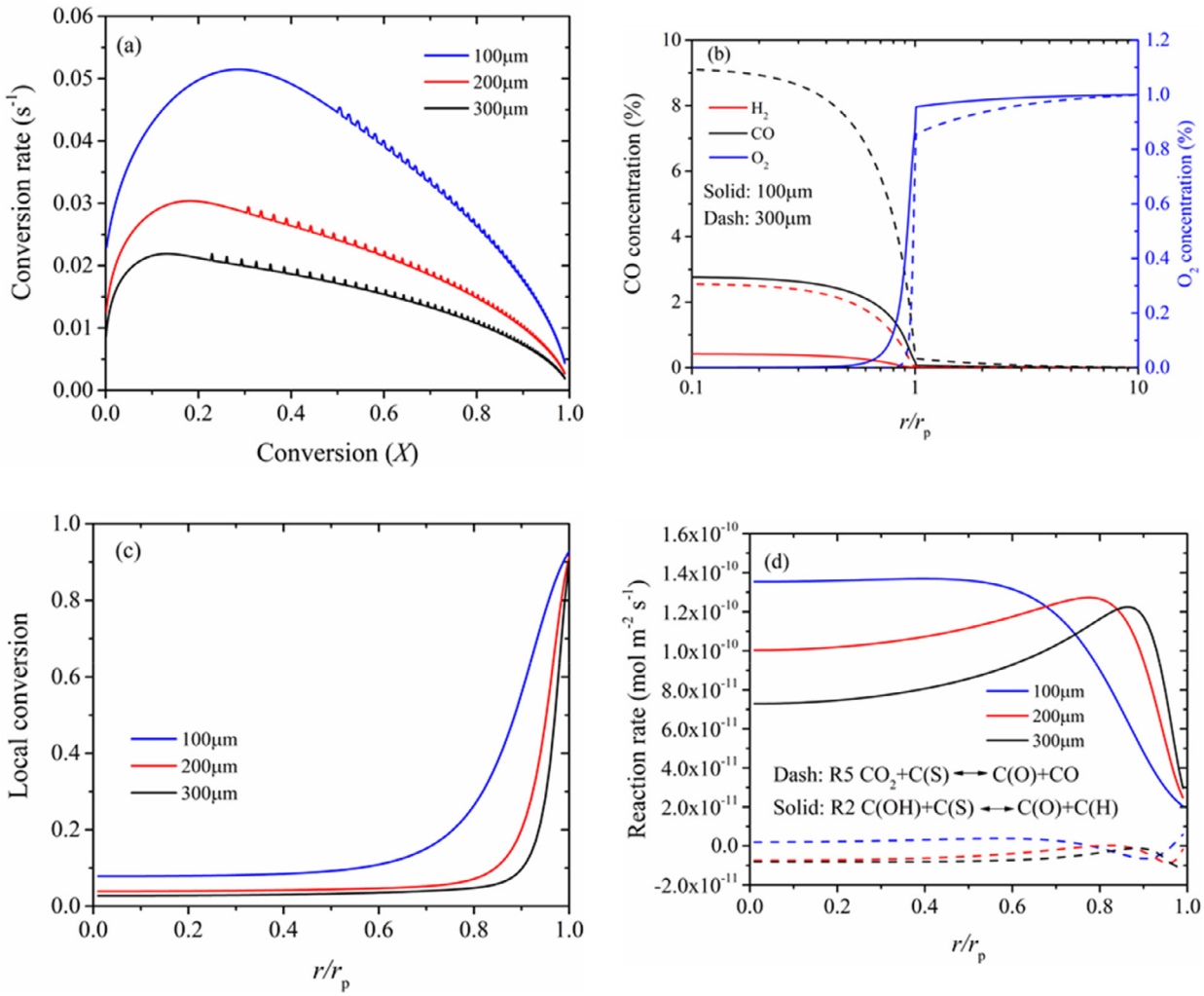

Fig. 9. Char conversion characteristics at different particle size at t = 8 s. (T_{gas} 1223 K, 1 vol.% O_2, 50 vol.% H_2O, 49 vol.% CO_2).

The influences of the O_2 concentration on the gasification reaction and char conversion inside the particle are also revealed. At a higher O_2 concentration, the oxidation reaction rate is faster and the heat generated from the exothermic oxidation reaction results in a higher particle temperature, as shown in Fig. 7b. However, even when the O_2 concentration reaches 4 vol.%, the reaction temperature is only 10 K higher than the ambient temperature. Therefore, it can be deduced that the influence of exothermic oxidation reaction on the particle temperature is limited under the investigated oxygen concentration range. As shown in Fig. 7c, for the same reaction time (t = 2.5 s), the local conversion of the inner region of the char particle at a high O_2 concentration is almost the same as that at a low O_2 concentration. This demonstrates that the increase of O_2 concentration does not accelerate the gasification reaction rate significantly from the aspect of increasing the char particle temperature. On the other side, with the increase of O_2 concentration, the penetration distance of O_2 increases (Fig. 7d). Nevertheless, the O_2 concentrations are still close to 0 inside most of the char particle. To sum up, the increase of O_2 concentration contributes little to the conversion of interior char, although it will undoubtedly accelerate the conversion of exterior char. As for the conditions studied in Fig. 7d, the penetration depth of O_2 can reach $0.2r_p$, and in this part of the solid domain, the pore surface area is hundreds of times of the particle external surface area. Therefore, it is reasonable to conclude that the contribution of the external surface to the heterogeneous reactions is weak.

3.4. The effects of steam concentration on char conversion rate

Figure 8 summarizes the results of a series of simulations, in which the concentrations of steam is varied over a wide range (10–99 vol.%) at a fixed O_2 concentration (1 vol.%) and using CO_2 as balance gas with char particle size of 100 μm at 1223 K. As the concentration of steam increases (CO_2 concentration decreases simultaneously), the conversion rate of char particle increases (Fig. 8a), and the particle temperature decreases slightly (about 1 K, not shown). Figure 8b shows the local conversion of char particle at t = 8 s. It can be found that the local conversion inside the char particle is gradually improved with the increase of steam concentration. However, at the particle surface, gasification reactions do not significantly improve the local conversion of coal char, which is mainly due to the relatively high O_2 concentration in this region as shown in Fig. 8c (main species distribution).

Another noteworthy point is the direction of CO_2 gasification reaction (R5: CO_2+C(S) ↔ C(O)+CO). Figure 8d shows the overall reaction rates of R5 (mol * s^{-1}) at t = 8 s under different H_2O concentrations. With the increase of H_2O concentration (or the decrease of CO_2 concentration), the overall reaction rate of R5 decreases. However, when the H_2O concentration reaches 70 vol.%

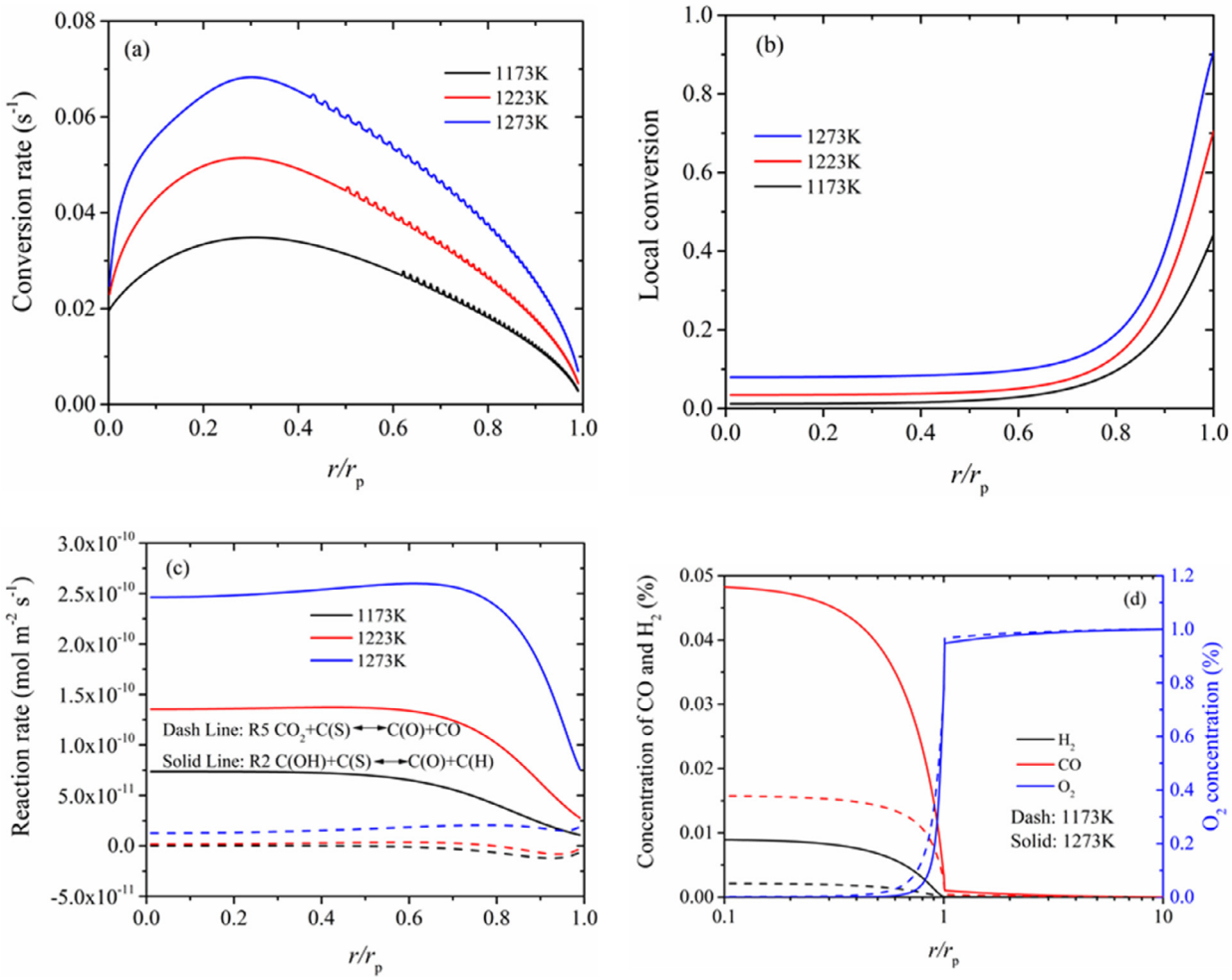

Fig. 10. Char conversion characteristics at different reaction temperature at t = 5.5 s. (d_p = 100 μm, 1 vol.% O_2, 50 vol.% H_2O, 49 vol.% CO_2).

(CO_2: 29 vol.%), the equilibrium of R5 shifts to the left side due to the increase of CO concentration (see Fig. 8c) and the decrease of CO_2 concentration. Consequently, the overall reaction rate of R5 becomes negative. The negative reaction rate of R5 will be further analyzed in Section 3.8.

3.5. The effects of particle size on char conversion rate

Simulations are also conducted for the conversion of char particle with different sizes. As shown in Fig. 9a, it is clear that the smaller char particle demonstrates a higher conversion rate. Actually, the char particle size can significantly affect the internal diffusion resistance of the reactants and products. For the smaller particle, the penetration depth of O_2 is relatively closer to the particle center as shown in Fig. 9b, which means that a higher proportion of the particle are dominated by the faster oxidation reaction, thus resulting in a higher conversion rate. In the meanwhile, the concentrations of steam and CO_2 (reactants) in the center of smaller char particle are higher (meaning a higher char gasification rate), while the concentrations of products (such as H_2 and CO) are lower due to the lower diffusion resistance. With the increase of particle diameter from 100 to 300 μm, the O_2 concentration at char particle surface only decrease from 0.959% to 0.857%, which can be explained by the fact that the carbon consumption rate (mol C per second) of large particle is higher than that of fine particle. Eventually, O_2 is consumed at a faster rate and resulting in a concentration gradient. The small difference of O_2 concentration at particle surface between the two particle sizes (0.959% for 100 μm and 0.857% for 300 μm) indicates that the impact of external diffusion on oxygen concentration is not significant. Figure 9c plots the local conversion at t = 8 s. At the exterior of the particle, the local conversion of bigger particle is much lower than that of smaller particle, which is mainly due to its low local O_2 concentration (then a lower oxidation rate). While inside the larger particle, the local conversion is still lower due to the shorter O_2 penetration depth (weaker oxidation) and the lower CO_2/H_2O concentration (weaker gasification). Meanwhile, the higher concentrations of H_2 and CO in the interior of larger particle (see Fig. 9b) have certain inhibiting effects on the gasification reaction [40]. In Fig. 9d, the reaction rates of R2 (steam-char gasification) and R5 (CO_2-char gasification) are plotted. It can be found that the gasification reactions in the particle center are faster for the smaller particle. Factually, along the radial direction, the H_2 (or CO) concentration is decreasing and the inhibition effect on steam-char gasification (or CO_2-char gasification) is weakened. Therefore, the gasification rates increase first from the inside to the outside of the char particle. However, when closing to the particle surface, the presence of O_2 inhibits the gasification reaction and slows down the gasification rate.

3.6. The effects of temperature on char conversion rate

Reaction temperature is also an important factor to affect the conversion rate of char. As can be anticipated, the char conver-

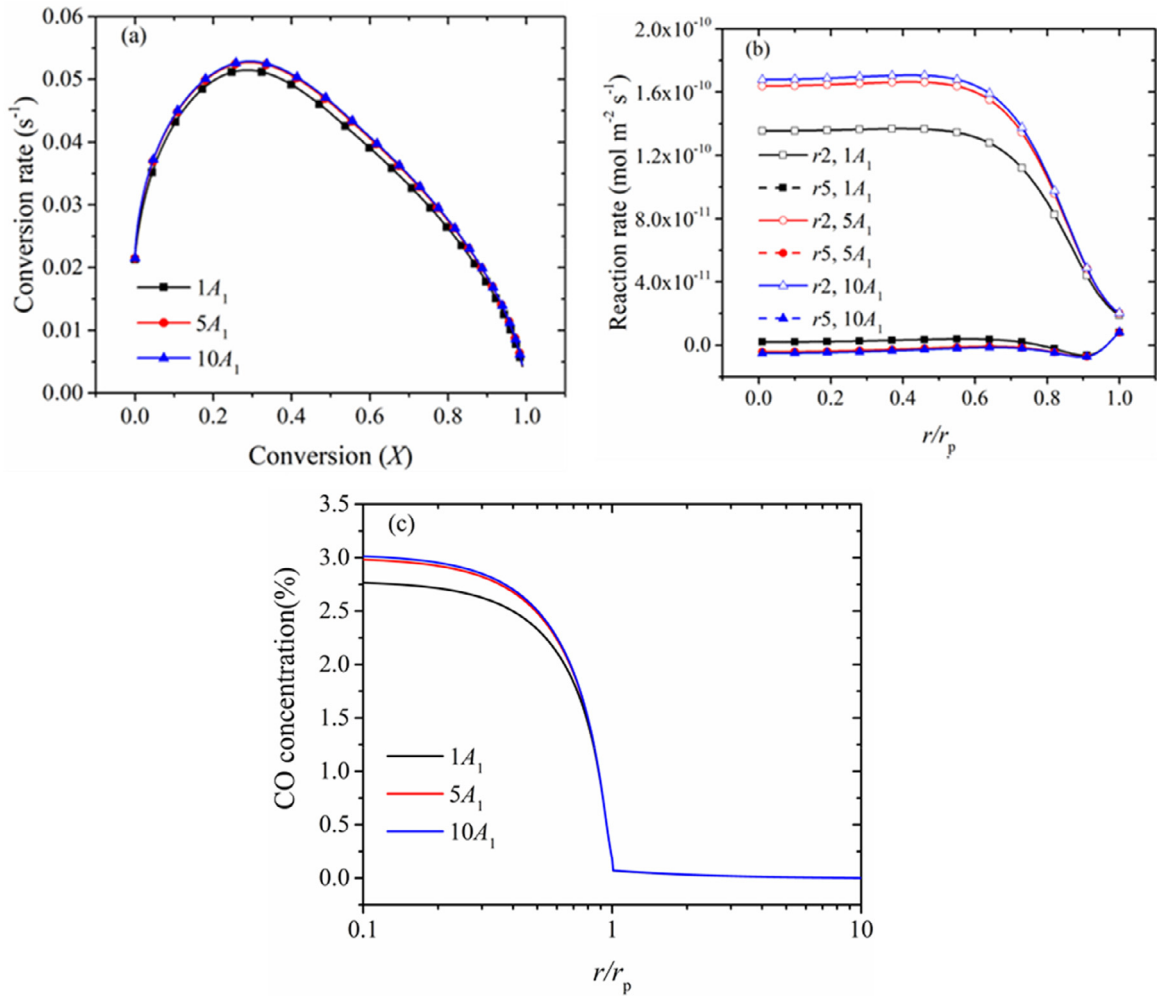

Fig. 11. The char conversion characteristics under varied pre-exponential factor of R1. d_p = 100 μm, T_{gas} = 1223 K, 1 vol.% O_2/50 vol.% H_2O/49 vol.% CO_2. The data in (b) and (c) correspond to t = 8 s.

sion rate increases significantly with the environment temperature (Fig. 10a). The internal and external local conversions of char particle both increase at a higher temperature, which indicate that the increase of temperature promotes the reaction rates of both gasification and oxidation. However, it should be noted that with the increase of gas temperature (from 1173 K to 1223 K), the local char conversion inside the particle (due to gasification reactions) is increased by 6 times, while the local char conversion in the external layer of the particle (due to oxidation) is only doubled, which indicates that gas temperature has a more significant effect on the gasification reaction rate. To be more specific, as the reaction temperature increases, the H_2O-char gasification is greatly accelerated, while the CO_2-char gasification rate is only slightly increased (see Fig. 10c). As shown in Fig. 10d, with the increase of gas temperature from 1173 to 1273 K, the O_2 concentration at char particle surface decreases from 0.967% to 0.947%. Therefore, it can be concluded that the gas temperature does not play an important role in the external diffusion effect under the investigated conditions.

3.7. Sensitivity analysis

The assessment of parametric sensitivity (including reaction mechanisms like reaction rate constant of R5 and char structural parameters like porosity) is essential for model accuracy validation, predictive power, and scientific finding inherent to simulation results. In this part, the sensitivity analyses of main heterogeneous reaction kinetics parameters and char particle physical properties are conducted, where the Wyodak coal char is simulated with the heterogeneous reaction kinetics in Table. 2 and the physical properties in Table. 5 for a reference case. All the simulations in this section are conducted at 1223 K, with 1% O_2/49% H_2O/49 CO_2, and d_p = 100 μm.

3.7.1. The sensitivity assessment of kinetics parameters of heterogeneous reactions

Firstly, to determine the effects of the H_2O gasification reaction (R1, the adsorption step of H_2O gasification) on the char conversion, other heterogeneous reaction and product distribution, its activation energy (E_1) is fixed and the pre-exponential factor, A_1, for the char gasification steps are varied in separate simulations. The results are shown in Fig. 11. With the increase of A_1, the char conversion is slightly accelerated. However, the increment of conversion rate is not obvious while A_1 is magnified from five times to ten times. As shown in Fig. 11b, however the reaction rate of R2 ($r2$) is greatly enhanced, while the reaction rate of R5 ($r5$) is slightly decreased (which suggests that the CO_2 gasification is inhibited). It may be contributed to the fact that the enhanced H_2O reaction increases the CO concentration as shown in Fig. 11c. It is noted that, along the direction of the radius, this inhibitive effect of H_2O adsorption on the CO_2 gasification is weakening, which corresponds to the trends of CO concentration.

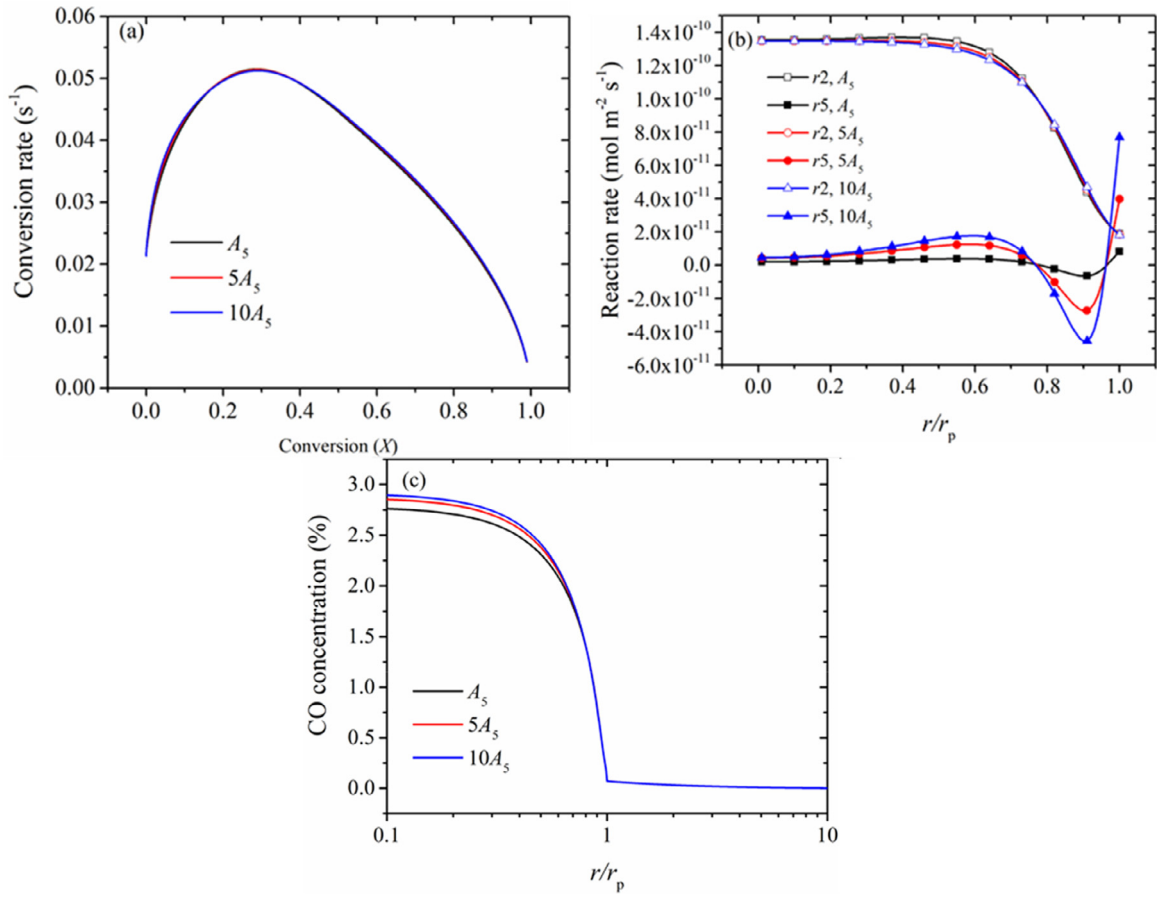

Fig. 12. The char conversion characteristics under varied pre-exponential factor of R5. d_p = 100 μm, T_{gas} = 1223 K, 1 vol.% O_2/50 vol.% H_2O/49 vol.% CO_2. The data in (b) and (c) correspond to t = 8 s.

The same treatment is applied to the sensitivity analysis of R5 (the adsorption step of CO_2 gasification), and the results are shown in Fig. 12. It seems that the CO_2 gasification has little effect on the char conversion as the pre-exponential factor of R5 (A_5) changes. Along the direction of the radius, the reaction rate of R5 ($r5$) firstly increases, which is ascribed to the lower CO concentration. While at the oxidation zone ($r/r_p > 0.7$), the fraction of surface species, C(O), is greatly increased, which facilitate the reverse reaction of R5. While approaching to the char particle surface ($r/r_p = 1$), the CO concentration is close to zero due to the oxidation reaction by O_2, therefore $r5$ increases again.

Note that the equilibrium constant of the reversible reaction R5 remains the same, although the pre-exponential factor is changed here. So, while we enlarge the pre-exponential factor several times (*e.g.*, β times), both the forward reaction rate of R5 ($r5^+$) and its reverse reaction rate ($r5^-$) are enhanced to $\beta \times r5^+$ and $\beta \times r5^-$ respectively. Therefore the overall reaction rate of R5 ($r5{=}\beta \times r5^+ - \beta \times r5^-$), which is either positive ($r/r_p \in [0, 0.77] \cup [0.96, 1]$) or negative ($r/r_p \in [0.77, 0.96]$), is also increased β times, as demonstrated in Fig. 12b.

3.7.2. The sensitivity assessment of char particle physical properties

The effects of the change of char particle porosity are examined and the simulation results are shown in Fig. 13. With the increase of char particle porosity, the conversion rate is slightly enhanced. For a higher porosity, the internal diffusion resistance of reactants is smaller, therefore the effectiveness factor is larger (see Fig. 13b). In this work, the pore size is calculated by: $r_{pore} = \frac{2rf\phi}{\rho_{ap}S} = \frac{2rf\phi}{\rho_{true}(1-\phi)S}$. It can be deduced that the pore size is increased with the increase of porosity, which is helpful for the internal diffusion of the reactants.

The effects of the initial specific surface area (S_0) on char conversion characteristics are examined and the simulation results are shown in Fig. 14. With the initial specific surface area S_0 halved, generally the char conversion rate is decreased. From Fig. 14b, it can be found that at the zone of $0.4 \le r/r_p \le 0.8$, the local conversion is higher for the case "$0.5S_0$". This is because the O_2 concentration for the case "$0.5S_0$" is higher than that for the case "S_0" at this zone, as shown in Fig. 14d. Combined with Fig. 14c, it can be found that under a smaller initial specific surface area, the gasification reaction inside the char particle is inhibited by the lean-O_2 oxidation reaction over a larger regime.

The effects of the active site density (Γ) on char conversion characteristics are also examined and the simulation results are shown in Fig. 15. Since the active site density can affect the adsorption of reactant molecules on the surface of char, the conversion rate of char decreases with the decrease of the active site density. Both the char oxidation reaction and gasification reaction rates slow down, as shown in Fig. 15c. And due to the lower oxidation reaction rate, the O_2 concentration inside the char particle is slighter higher for a smaller active site density.

3.8. Relative contributions to carbon consumption by steam gasification and CO_2 gasification

The relative contributions of CO_2 and steam gasification to the overall carbon conversion are plotted in Fig. 16. With the increase of O_2 concentration, the relative contributions of gasification reactions are reduced. According to the results shown in Fig. 7b, the

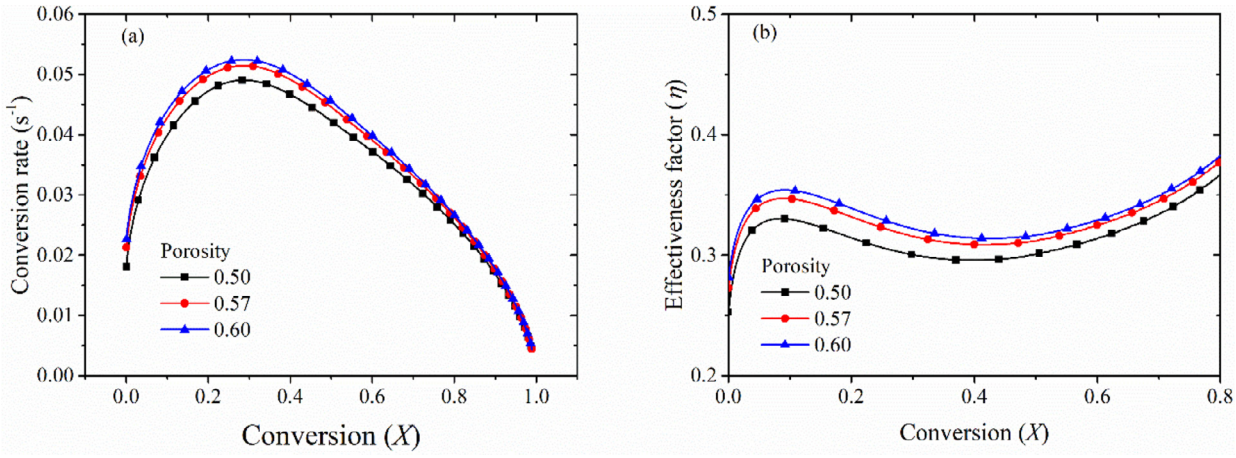

Fig. 13. The char conversion characteristics for three different porosity. d_p=100 μm, T_{gas} = 1223 K, 1 vol.% O_2/50 vol.% H_2O/49 vol.% CO_2. The true density is 1302 kg/m^3 for all three cases.

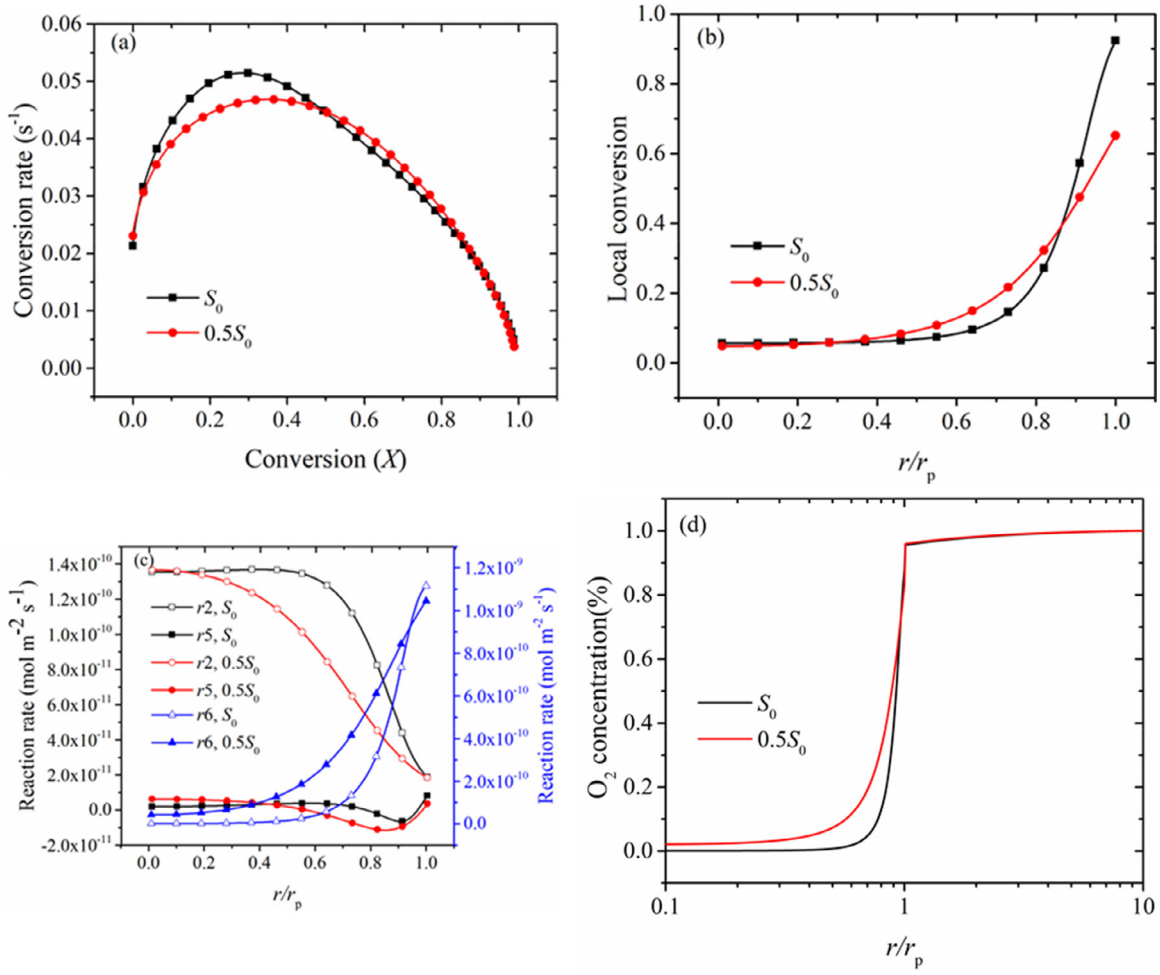

Fig. 14. The char conversion characteristics for different initial specific surface areas. d_p = 100 μm, T_{gas} = 1223 K, 1 vol.% O_2/50 vol.% H_2O/49 vol.% CO_2.

effect of O_2 concentration on the particle temperature is minimal. With the increase of O_2 concentration, the char particle burn-out time decreases significantly, but the gasification rate does not increase too much due to the slight increase of particle temperature, which results in the decrease of the gasification contribution. Furthermore, a higher O_2 concentration may inhibit the gasification reaction over a larger area. To sum up, these effects make the contribution of gasification reaction less at higher O_2 concentrations.

Figure 16b shows the relative contributions of gasification reactions when varying the steam concentration between 10 and 99 vol.% (CO_2 as balance gas). With the increase of steam concentration (accordingly the CO_2 concentration decrease in these simulations), the contribution of H_2O increases but that of CO_2 decreases as expected. However, when the steam concentration reaches 70 vol.%, the reaction rate of R5 is negative (as analyzed in Fig. 8d), which results in a negative value for the contribution

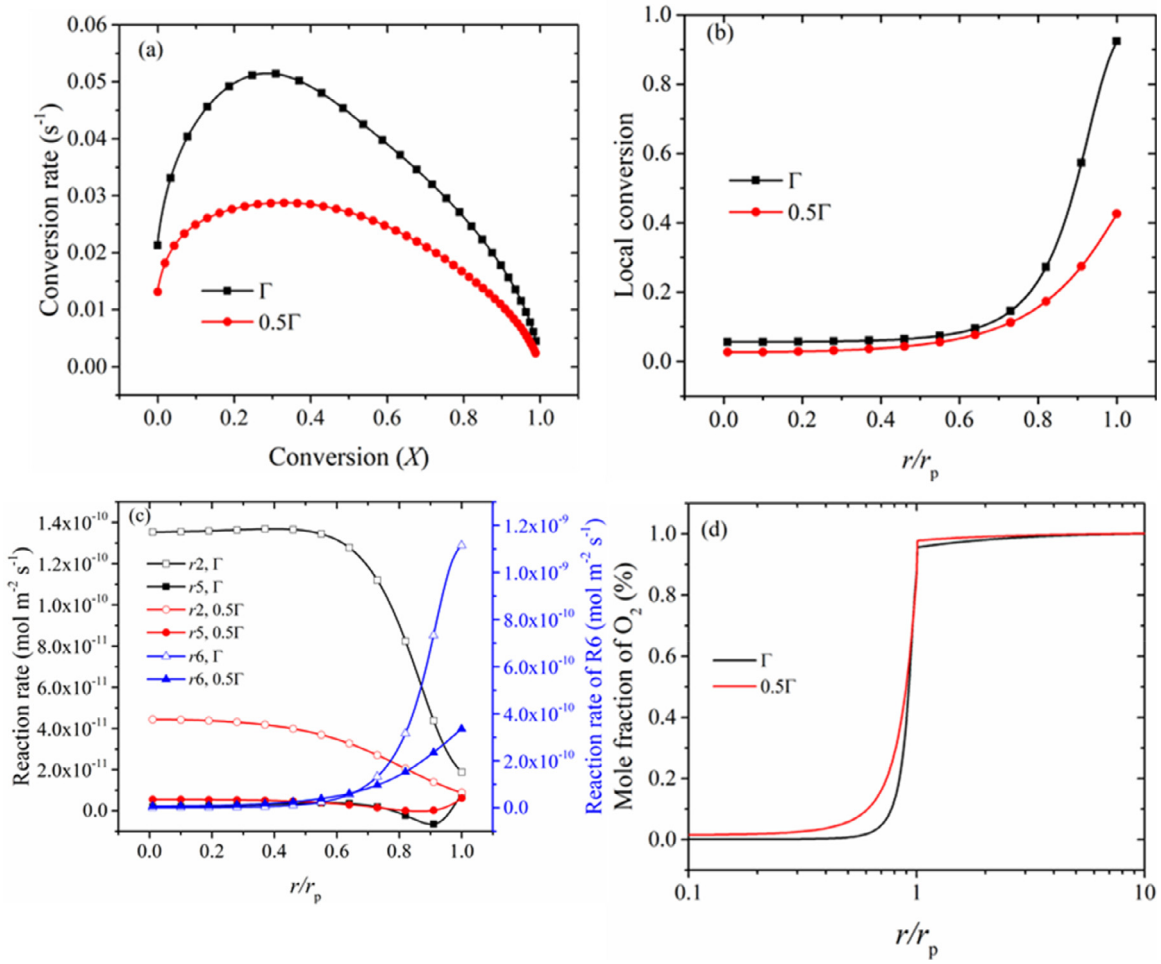

Fig. 15. The char conversion characteristics for different active site density. d_p = 100 μm, T_{gas} = 1223 K, 1 vol.% O_2/50 vol.% H_2O/49 vol.% CO_2.

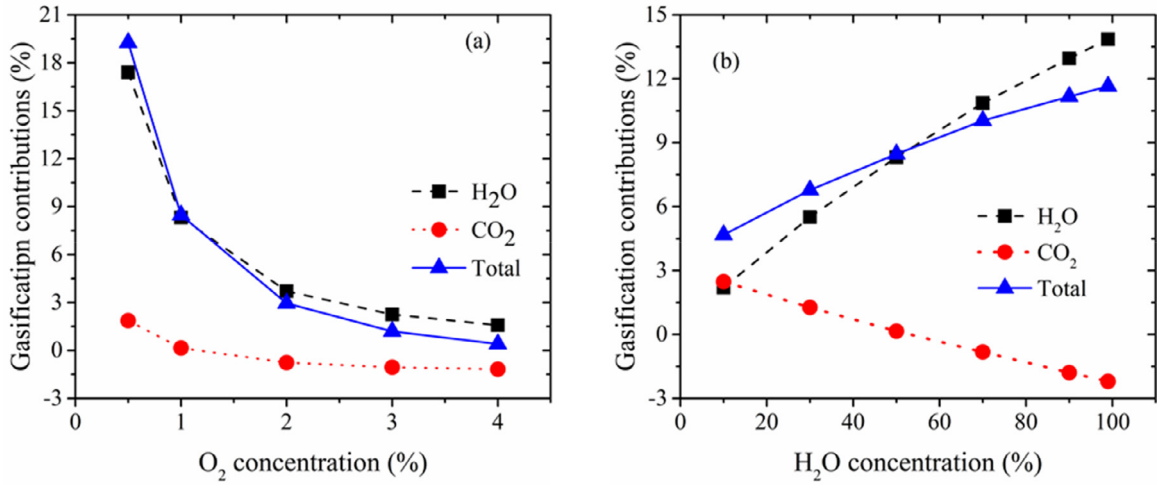

Fig. 16. Relative contribution degree of gasification reactions to the overall carbon consumption under different O_2 (a) and steam (b) concentrations. The total gasification contribution is the sum of H_2O and CO_2 gasification contributions.

of char-CO_2 gasification according to the calculation Eq. (6). When calculating the relative contributions of CO_2/steam gasification to the overall char conversion, we first calculate the amounts of C(O) generated by char reacting with CO_2 (R5) and steam (R2). However, both R2 and R5 are reversible reactions, which means that C(O) may be generated as a result of normal char gasification reaction or be consumed as the result of the reverse reaction. In the simulation, both the normal gasification and its reverse reaction work automatically. At 70 vol.% of steam concentration, the reverse reaction (C(O)+CO → CO_2+C(S)) prevails over the normal CO_2-char gasification (CO_2+C(S) → C(O)+CO)). As a result, the amount of C(O) generated through R5 will be negative and the relative contribution of CO_2-char gasification becomes negative. Nevertheless, it is worth noting that the presence of CO_2 is still conducive to

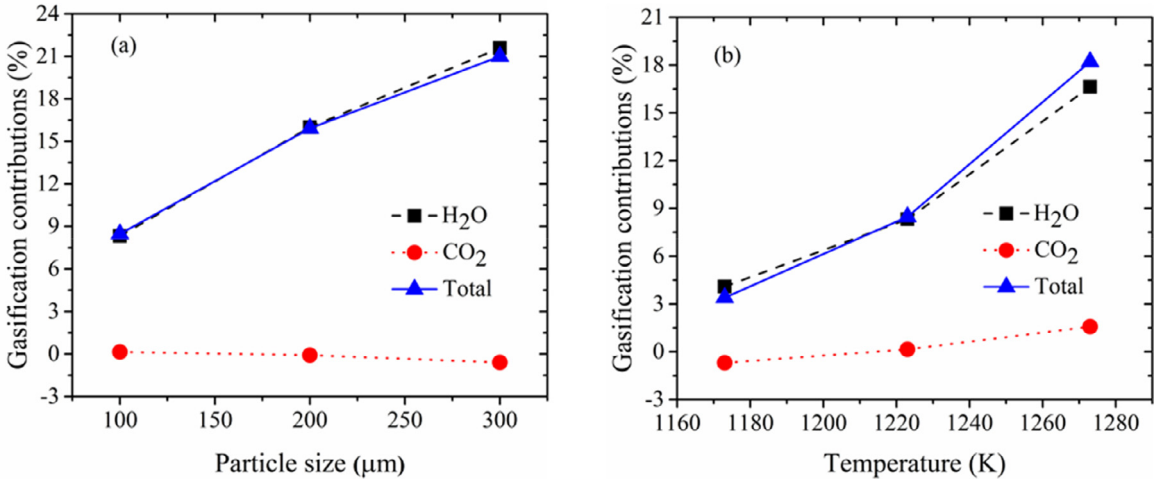

Fig. 17. Relative contributions of oxidation and gasification reactions to the overall carbon consumption under different particle sizes (a) and temperatures (b). The total gasification contribution is the sum of H_2O and CO_2 gasification contributions.

the conversion of coal char to some extent, by reducing the reverse reaction rate of R5 (which cannot be quantified in this work). With the increase of O_2 concentration, the same phenomenon occurs (negative value for the rate of R5), mainly because more CO and C(O) are produced inside the particle (at 1223 K, oxidation reaction also produces CO_2, but mainly CO).

Figure 17 presents the contributions of gasification reactions under different ambient temperatures and particle sizes. The changes in the relative contributions for both gasification agents (CO_2 and H_2O) have the same tendency at different particle sizes, and generally the CO_2 and H_2O gasification reactions play a more important role for larger char particles (Fig. 17a) [41]. As discussed above, due to the high reactivity of O_2 towards carbon matrix, O_2 could preferentially adsorb at the active sites and occupy the sites (as described by kinetics parameters of heterogeneous reactions), thus inhibiting the gasification reactions. Therefore, gasification reactions mainly occur in the zone where the O_2 concentration is close to 0. For the char particle with different sizes, the penetration depth of O_2 is nearly the same (in fact, it is slightly deeper for smaller particle), which allows the larger particle to have a bigger gasification area (as can be seen in Fig. 9b), and so as to attain a higher gasification contribution.

As the gas temperature increases, both oxidation and gasification reactions are facilitated. However, according to the results of the local char conversion shown in Fig. 10b, it can be inferred that the improvement of gasification reaction is higher than that of the oxidation reaction (more specifically, the rate of the CO_2/H_2O gasification reaction is more sensitive to temperature than the oxidation rate due to the higher activation energy). Therefore, the relative contributions of both gasification agents increase with the increase of reaction temperature, especially for the contribution of steam gasification (Fig. 17b).

In this work, the coal selected in this work is the Wyodak coal, a low-ash, sub-bituminous coal from Wyoming. If a high rank coal char (*e.g.* anthracite) is used in this study, the simulation results will be different quantitatively as the pore structure and chemical reactivity of coal char with $O_2/H_2O/CO_2$ are greatly different (even in the same conditions). The parametric sensitivity analysis shown in Section 3.7 also provide the information more or less. It can be expected that the decreased reactivity and porosity of the high rank coal char will result in a decreased gasification relative contribution, because the overall reaction rate of gasification is more sensitive to the porosity in comparison to that of the oxidation.

4. Conclusions

In this work, the particle-resolved simulation is conducted to investigate the effects of temperatures, char sizes, and gas compositions on char conversion characteristics under typical CLOU conditions (low O_2 concentration and high CO_2/steam concentration). Based on the detailed heterogeneous and homogeneous reaction mechanism, the contributions of H_2O/CO_2 gasification to the overall char conversion are analyzed. The following conclusions can be drawn from this study:

(1) The existence of gasification reactions will only reduce the char particle temperature at a very small degree (about 1 K) and shows a weak influence on the external diffusion of O_2. Therefore, it can be concluded that the influence of gasification on oxidation under CLOU conditions are minimal.
(2) O_2 can preferentially occupy the active sites at the surface of char particle, which inhibits the exterior gasification reaction. Consequently, the gasification reactions mainly occur inside the particle, where the oxidation reaction is almost negligible.
(3) The gasification reaction inside the char particle is mainly dominated by steam gasification. The contribution of CO_2 to overall char conversion is mainly reflected by inhibiting the reverse reaction of char-CO_2 gasification, rather than directly participating in the conversion of char particle (consuming C(B) and generating C(O)).
(4) The total contribution of gasification reactions to the overall char conversion is between 1 and 20% for the conditions studied and the char selected in this paper, which depends on the ambient temperature, gas composition, and particle size. And with the increase of O_2 concentration or the decrease of gasification agent concentration, temperature and char size, the contribution of the gasification reactions will decrease significantly.

In the current simulation, some simplifications have been made on the aspect of the conversion environment of char particle. Indeed, such simplifications constitute the weakness of the model. For example, the effects of fragmentation and attrition caused by collisions between particle and particle/wall in fluidized beds are not considered. Furthermore, as the char particle is considered as an ash-free carbon particle, the potential effects of the ash layer adhering on the char particle surface to affect the resistance of gas diffusion are not taken into account. Therefore, future work

should be devoted to the coupling of more realistic processes into the single-particle model and to the development of a CFD simulation applicable model based on the particle-resolved simulations [42].

Declaration of Competing Interest

The authors declare that they have no known competing financial interests or personal relationships that could have appeared to influence the work reported in this paper.

Acknowledgments

This work was supported by "National Key R&D Program of China (2016YFB0600801)" and "National Natural Science Foundation of China (52025063)".

References

[1] J. Adanez, A. Abad, F. Garcia-Labiano, P. Gayan, L.F. de Diego, Progress in chemical-looping combustion and reforming technologies, Prog. Energ. Combust. 38 (2012) 215–282.
[2] H. Zhao, X. Tian, J. Ma, M. Su, B. Wang, D. Mei, Development of tailor-made oxygen carriers and reactors for chemical looping processes at Huazhong University of Science & Technology, Int. J. Greenh. Gas Con. 93 (2020) 1028–1098.
[3] H. Zhao, X. Tian, J. Ma, X. Chen, M. Su, C. Zheng, Y. Wang, Chemical looping combustion of coal in china: comprehensive progress, remaining challenges, and potential opportunities, Energy Fuels 34 (2020) 6696–6734.
[4] J. Adánez, A. Abad, T. Mendiara, P. Gayán, L.F. de Diego, F. García-Labiano, Chemical looping combustion of solid fuels, Prog. Energ. Combust. 65 (2018) 6–66.
[5] A. Lyngfelt, Chemical-looping combustion of solid fuels – Status of development, Appl. Energy 113 (2014) 1869–1873.
[6] A. Shulman, E. Cleverstam, T. Mattisson, A. Lyngfelt, Manganese/Iron, Manganese/Nickel, and Manganese/Silicon oxides used in chemical-looping with oxygen uncoupling (CLOU) for combustion of methane, Energy Fuels 23 (2009) 5269–5275.
[7] X. Tian, M. Su, H. Zhao, Kinetics of redox reactions of $CuO@TiO_2$–Al_2O_3 for chemical looping combustion and chemical looping with oxygen uncoupling, Combust. Flame 213 (2020) 255–267.
[8] D.G. Roberts, D.J. Harris, Char gasification with O_2, CO_2, and H_2O: effects of pressure on intrinsic reaction kinetics, Energy Fuels 14 (2000) 483–489.
[9] T. Mattisson, A. Lyngfelt, H. Leion, Chemical-looping with oxygen uncoupling for combustion of solid fuels, Int. J. Greenh. Gas Con. 3 (2009) 11–19.
[10] K. Wang, H. Zhao, X. Tian, Y. Fang, J. Ma, C. Zheng, Chemical-looping with oxygen uncoupling of different coals using copper ore as an oxygen carrier, Energy Fuels 29 (2015) 6625–6635.
[11] J. Brix, P.A. Jensen, A.D. Jensen, Coal devolatilization and char conversion under suspension fired conditions in O_2/N_2 and O_2/CO_2 atmospheres, Fuel 89 (2010) 3373–3380.
[12] J.J. Murphy, C.R. Shaddix, Combustion kinetics of coal chars in oxygen-enriched environments, Combust. Flame 144 (2006) 710–729.
[13] C.R. Shaddix, E.S. Hecht, C. Gonzalo-Tirado, B.S. Haynes, The effect of bulk gas diffusivity on apparent pulverized coal char combustion kinetics, Proc. Combust. Inst. 37 (2019) 3071–3079.
[14] A. Molina, C.R. Shaddix, Ignition and devolatilization of pulverized bituminous coal particles during oxygen/carbon dioxide coal combustion, Proc. Combust. Inst. 31 (2007) 1905–1912.
[15] F. Normann, K. Andersson, B. Leckner, F. Johnsson, Emission control of nitrogen oxides in the oxy-fuel process, Prog. Energ. Combust. 35 (2009) 385–397.
[16] C. Yin, J. Yan, Oxy-fuel combustion of pulverized fuels: combustion fundamentals and modeling, Appl. Energy 162 (2016) 742–762.
[17] T. Maffei, R. Khatami, S. Pierucci, T. Faravelli, E. Ranzi, Y.A. Levendis, Experimental and modeling study of single coal particle combustion in O_2/N_2 and Oxy-fuel (O_2/CO_2) atmospheres, Combust. Flame 160 (2013) 2559–2572.
[18] E.S. Hecht, C.R. Shaddix, A. Molina, B.S. Haynes, Effect of CO_2 gasification reaction on oxy-combustion of pulverized coal char, Proc. Combust. Inst. 33 (2011) 1699–1706.
[19] E.S. Hecht, C.R. Shaddix, M. Geier, A. Molina, B.S. Haynes, Effect of CO_2 and steam gasification reactions on the oxy-combustion of pulverized coal char, Combust. Flame 159 (2012) 3437–3447.
[20] D. Kim, S. Choi, C.R. Shaddix, M. Geier, Effect of CO_2 gasification reaction on char particle combustion in oxy-fuel conditions, Fuel 120 (2014) 130–140.
[21] H. Tolvanen, R. Raiko, An experimental study and numerical modeling of combusting two coal chars in a drop-tube reactor: a comparison between N_2/O_2, CO_2/O_2, and $N_2/CO_2/O_2$ atmospheres, Fuel 124 (2014) 190–201.
[22] S.R. Dhaneswar, S.V. Pisupati, Oxy-fuel combustion: the effect of coal rank and the role of char-CO_2 reaction, Fuel Process. Technol. 102 (2012) 156–165.
[23] J. Brix, P.A. Jensen, A.D. Jensen, Modeling char conversion under suspension fired conditions in O_2/N_2 and O_2/CO_2 atmospheres, Fuel 90 (2011) 2224–2239.
[24] C. Gonzalo-Tirado, S. Jiménez, R. Johansson, J. Ballester, Comparative study of four alternative models for CO oxidation around a burning coal char particle, Combust. Flame 161 (2014) 1085–1095.
[25] Y. Li, R. Sun, M. Wang, Z. Wang, J. Xu, X. Ren, Reaction kinetics of char-O_2/H_2O combustion under high-temperature entrained flow conditions, Fuel 243 (2019) 172–184.
[26] H. Zhou, Y. Li, N. Li, K. Cen, Experimental investigation of ignition and combustion characteristics of single coal and biomass particles in O_2/N_2 and O_2/H_2O, J. Energy Inst. 92 (2019) 502–511.
[27] L. Chen, S.Z. Yong, A.F. Ghoniem, Oxy-fuel combustion of pulverized coal: characterization, fundamentals, stabilization and CFD modeling, Prog. Energ. Combust. 38 (2012) 156–214.
[28] I. Adánez-Rubio, P. Gayán, A. Abad, F. García-Labiano, L.F. de Diego, J. Adánez, Kinetic analysis of a Cu-based oxygen carrier: relevance of temperature and oxygen partial pressure on reduction and oxidation reactions rates in Chemical Looping with Oxygen Uncoupling (CLOU), Chem. Eng. J. 256 (2014) 69–84.
[29] C.K. Clayton, K.J. Whitty, Measurement and modeling of decomposition kinetics for copper oxide-based chemical looping with oxygen uncoupling, Appl. Energy 116 (2014) 416–423.
[30] M. Su, X. Tian, H. Zhao, Particle-resolved simulation and modeling of the conversion rate of coal char in chemical looping with oxygen uncoupling, Combust. Flame 213 (2020) 331–342.
[31] M.B. Tilghman, R.E. Mitchell, Coal and biomass char reactivities in gasification and combustion environments, Combust. Flame 162 (2015) 3220–3235.
[32] G.P. Smith, S.D. Golden, M. Frenklach, N.W. Moriarty, B. Eitener, M. Goldenberg, C.T. Bowman, R.K. Hanson, S. Song, W.C. Gardiner, V.V. Lissianski, Z. Qin, GRIMech 3.0, 2001. http://www.me.berkeley.edu/gri_mech.
[33] L. Ma, Ph.D. Thesis, Mechanical Engineering Department, Stanford University, Palo Alto, CA, 2006.
[34] R.E. Mitchell, L. Ma, B. Kim, On the burning behavior of pulverized coal chars, Combust. Flame 151 (2007) 426–436.
[35] S.K. Bhatia, D.D. Perlmutter, A Random Pore Model for Fluid-Solid Reactions: I. Isothermal, Kinetic Control, AIChE Journal 26 (1980) 379–386.
[36] N.E.L. Haugen, R.E. Mitchell, M.B. Tilghman, A comprehensive model for char particle conversion in environments containing O_2 and CO_2, Combust. Flame 162 (2015) 1455–1463.
[37] O. Karlström, A. Brink, M. Hupa, Desorption kinetics of CO in char oxidation and gasification in O_2, CO_2 and H_2O, Combust. Flame 162 (2015) 788–796.
[38] T.R. Marrero, E.A. Mason, Gaseous Diffusion Coefficients, J. Phys. Chem. Ref. Data 1 (1972) 3–118.
[39] F. Scala, Fluidized bed gasification of lignite char with CO_2 and H_2O: a kinetic study, Proc. Combust. Inst. 35 (2015) 2839–2846.
[40] Z. Huang, J. Zhang, Y. Zhao, H. Zhang, G. Yue, T. Suda, M. Narukawa, Kinetic studies of char gasification by steam and CO_2 in the presence of H_2 and CO, Fuel Process. Technol. 91 (2010) 843–847.
[41] O. Karlström, L. Hupa, Energy conversion of biomass char: oxidation rates in mixtures of $O_2/CO_2/H_2O$, Energy 181 (2019) 615–624.
[42] M. Su, H. Zhao, A modified intrinsic model for conversion rate of coal char particle in chemical looping with oxygen uncoupling conditions, Fuel 288 (2021) 119615.